JOURNAL OF COMPUTATIONAL PHYSICS **128,** 181–196 (1996)
ARTICLE NO. 0202

A Second-Order Iterative Implicit–Explicit Hybrid Scheme for Hyperbolic Systems of Conservation Laws

WENLONG DAI AND PAUL R. WOODWARD

University of Minnesota, 116 Church Street S.E. Minneapolis, Minnesota 55455

Received November 13, 1995; revised April 9, 1996

An iterative implicit–explicit hybrid scheme is proposed for hyperbolic systems of conservation laws. Each wave in a system may be implicitly, or explicitly, or partially implicitly and partially explicitly treated depending on its associated Courant number in each numerical cell, and the scheme is able to smoothly switch between implicit and explicit calculations. The scheme is of Godunov-type in both explicit and implicit regimes, is in a strict conservation form, and is accurate to second-order in both space and time for all Courant numbers. The computer code for the scheme is easy to vectorize. Multicolors proposed in this paper may reduce the number of iterations required to reach a converged solution by several orders for a large time step. The feature of the scheme is shown through numerical examples.

1. INTRODUCTION

During the past two decades, Godunov schemes for hyperbolic systems of conservation laws have been developed which are particularly efficient for shock problems. Godunov [1] supposed that the initial data could be replaced by a set of piecewise constant data with discontinuities and used exact solutions of Riemann problems to advance piecewise constant data. A major extension to Godunov's scheme was made by Van Leer in his MUSCL scheme [2, 3] which used a Riemann solver to advance piecewise linear data. Other examples of Godunov schemes include Roe's method [4], the piecewise parabolic method (PPM) [5, 6], and the TVD method [7]. The essential ingredients of Godunov schemes include the use of characteristic formulations and an approximate Riemann solver which is suitable for computing a set of time-averaged fluxes at interfaces between grid cells.

Godunov schemes may be second-order accurate, but are explicit in time. A time step in an explicit scheme is restricted by the largest of Courant numbers associated with all kinds of waves, which cannot be larger than unity. For some problems described by a hyperbolic system of conservation laws, desired numerical schemes should be stable for large time steps and yet resolve shock fronts accurately if necessary. Schemes with this feature are more desired for a system in which different waves may have significantly different wave speeds. For those phenomena mainly associated with waves which have relatively small wave speeds, a small time step in an explicit scheme is one of the main restrictions which limits the efficiency of an explicit scheme in a simulation.

Implicit and implicit–explicit hybrid schemes for fluid dynamics have been developed for many years [8–22]. Beam and Warming [10] proposed an implicit scheme for hyperbolic systems of conservation laws. Engquist and Osher [11] proposed a method for transonic flows. Van Leer and Mulder [12] developed a scheme which is time-accurate for small time steps and turns into a relaxation method for large time steps. Yee *et al.* [13] proposed an implicit TVD scheme for steady states. Glaz and Wardlaw [14] proposed a high-order Godunov scheme for steady supersonic gas dynamics. Fryxell *et al.* [15] developed a method which extends Godunov schemes into the implicit regime. Jameson and Yoon [16, 17] proposed an implicit scheme which was combined with the multigrid method. More recently, Loh and Hui [18] developed a first-order Godunov scheme for steady supersonic flows; Blunt and Rubin [19] extended TVD schemes to fully implicit and partially implicit regimes; Wilcoxson and Manousiouthankis [20] developed an implicit time marching implementation of an essentially non-oscillatory scheme. Collins *et al.* [21] developed an implicit–explicit Eulerian Godunov scheme for compressible flows using a modified Enguist–Osher flux function. Dai and Woodward developed an iterative approach for implicit–explicit hybrid calculations for the Euler equations [22].

The Newton iteration is often used in implicit schemes for a nonlinear system. But, the Newton iteration is time-consuming in an implicit scheme. An implicit scheme typically involves linearization to get a linear system. The linear system is then exactly or approximately solved. An exact linear solver is difficult to vectorize and needs large memory. Therefore, iterative linear solvers are often used. But iterative solvers often need a large number of iterations. In this paper, a high-order implicit–explicit hybrid scheme for hyperbolic systems of conservation laws is developed,

0021-9991/96 $18.00

which is the extension of the approach reported in [22] to general systems. The iterative approach to be presented in this paper will result in a faster convergence than that reported in [22]. The iterative approach involves only a single level of iterations which solve both the implicit relations arising from upstream centered differences for all wave families and the nonlinearity of the systems. Only a small number of iterations is expected to be needed in a simulation with large time steps. The scheme is of Godunov-type in both implicit and explicit regimes and is expected to be able to resolve discontinuities.

The plan of this paper is as follows. The second section is an illustration of the scheme through linear advection. The scheme for hyperbolic systems of conservation laws is in the third section. The numerical examples for the Euler equations and ideal magnetohydrodynamical (MHD) equations are in the fourth section. The final section is for conclusions and a brief discussion.

2. A LINEAR ADVECTION SCHEME

We first illustrate the iterative implementation for linear advection

$$\frac{\partial a}{\partial t} + c\frac{\partial a}{\partial x} = 0, \tag{1}$$

where x and t are the space and time coordinates, a is the quantity being advected, and c is a constant advection velocity. Considering a numerical cell $[x_i, x_{i+1}]$, we write Eq. (1) in a difference form:

$$\langle a\rangle_i^{(n)} = \langle a\rangle_i - \frac{c\,\Delta t}{\Delta x_i}(\bar{a}_{i+1} - \bar{a}_i). \tag{2}$$

Here Δx_i is the width of the cell, Δt is the time step, $\langle a\rangle_i^{(n)}$ (or $\langle a\rangle_i$) is the cell-average of a over the cell at $t = \Delta t$ (or $t = 0$), and $\bar{a}_i$ is the time-average of a at x_i over the time step, i.e.,

$$\langle a\rangle_i^{(n)} \equiv \frac{1}{\Delta x_i}\int_{x_i}^{x_{i+1}} a(x, \Delta t)\,dx,$$

$$\bar{a}_i \equiv \frac{1}{\Delta t}\int_0^{\Delta t} a(x_i, t)\,dt.$$

For the case in which the Courant number σ_i ($\equiv c\,\Delta t/\Delta x_i$) is less than unity (Fig. 1a), the time-average $\bar{a}_{i+1}$ is equal to the domain-average of a over the domain of dependence $[x_{i+1} - c\,\Delta t, x_{i+1}]$, and the scheme is unconditionally stable.

For the case in which the Courant number is greater than unity, the domain of dependence extends beyond a cell interface, and thus the time-average $\bar{a}_{i+1}$ can not be calculated from the distribution of a over the neighbor cell. In this case, Fryxell *et al.* [15] introduced an extra time level at $t = \Delta t/2$ (Fig. 1b).

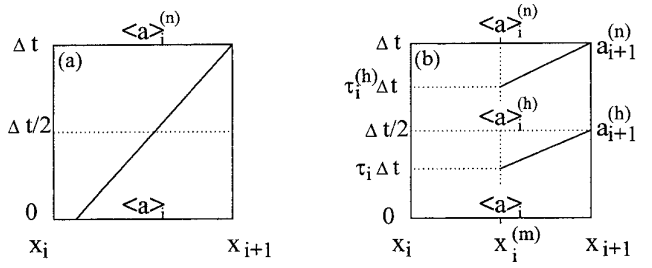

FIG. 1. The structure of a cell in space-time for two kinds of situations, one with the Courant number less than unity (a) and the other with the number greater than unity (b). In the first case, the time average of $a(x, t)$ over the time step Δt at x_{i+1} is equal to the spatial average of a over the domain $[x_{i+1} - c\,\Delta t, x_{i+1}]$ at $t = 0$. In the other case, an extra time level at $t = \Delta t/2$ is introduced, and two characteristics passing through $(x_{i+1}, \Delta t/2)$ or $(x_{i+1}, \Delta t)$ are traced back to the center $x_i^{(m)}$ of the cell.

For the first half time step, we have an equation similar to Eq. (2):

$$\langle a\rangle_i^{(h)} = \langle a\rangle_i - \frac{c\,\Delta t}{2\,\Delta x_i}(\bar{a}_{i+1}^{(h)} - \bar{a}_i^{(h)}). \tag{3}$$

Here $\langle a\rangle_i^{(h)}$ is the cell-average of a at $t = \Delta t/2$, and $\bar{a}_i^{(h)}$ is the time-average of a over the first half time step at $x = x_i$. The time-averages, $\bar{a}_i$ and $\bar{a}_i^{(h)}$, may be approximately calculated through a linear interpolation in time. The linear interpolation is uniquely determined by $a_i^{(h)}$ [$\equiv a(x_i, \Delta t/2)$] and $a_i^{(n)}$ [$\equiv a(x_i, \Delta t)$]. Thus, Eqs. (2), (3) may be written as

$$\langle a\rangle_i^{(n)} = \langle a\rangle_i - \sigma_i(a_{i+1}^{(h)} - a_i^{(h)}), \tag{4}$$

$$\langle a\rangle_i^{(h)} = \langle a\rangle_i - \tfrac{1}{2}\sigma_i[\tfrac{3}{2}a_{i+1}^{(h)} - \tfrac{1}{2}a_{i+1}^{(n)} - (\tfrac{3}{2}a_i^{(h)} - \tfrac{1}{2}a_i^{(n)})]. \tag{5}$$

We mention that fractional time step difference approximations have been used in [23, 24].

In order to find $a_{i+1}^{(n)}$ and $a_{i+1}^{(h)}$, two characteristic curves passing through $(x_{i+1}, \Delta t)$ or $(x_{i+1}, \Delta t/2)$ in the $(x - t)$-space are traced back to the center of the cell, $x_i^{(m)} \equiv (x_{i+1} + x_i)/2$ (see Fig. 1b). $a_{i+1}^{(n)}$ and $a_{i+1}^{(h)}$ are equal to $a(x_i^{(m)}, \tau_i^{(h)}\,\Delta t)$ and $a(x_i^{(m)}, \tau_i\,\Delta t)$ respectively. Here $\tau_i^{(h)}$ and τ_i are defined as

$$\tau_i^{(h)} \equiv 1 - \frac{1}{2\sigma_i}, \qquad \tau_i \equiv \frac{1}{2}\left(1 - \frac{1}{\sigma_i}\right).$$

Up to second order of accuracy, $a(x_i^{(m)}, \tau_i^{(h)}\,\Delta t)$ and $a(x_i^{(m)}, \tau_i\,\Delta t)$ are the cell-averages of a over the cell $[x_i, x_{i+1}]$ at $t = \tau_i^{(h)}\,\Delta t$ and $t = \tau_i\,\Delta t$ respectively, which may

be approximately calculated through a parabolic interpolation for the cell-average $\langle a\rangle_i$ (t) in time. The parabola is uniquely determined by three cell-averages, $\langle a\rangle_i$, $\langle a\rangle_i^{(h)}$, and $\langle a\rangle_i^{(n)}$. Therefore $a_{i+1}^{(n)}$ and $a_{i+1}^{(h)}$ may be written as

$$a_{i+1}^{(n)} = \langle a\rangle_i + (-\delta a_i^{(n)} + 4\,\delta a_i^{(h)})\tau_i^{(h)} + (2\,\delta a_i^{(n)} - 4\,\delta a_i^{(h)})(\tau_i^{(h)})^2, \tag{6}$$

$$a_{i+1}^{(h)} = \langle a\rangle_i + (-\delta a_i^{(n)} + 4\,\delta a_i^{(h)})\tau_i + (2\,\delta a_i^{(n)} - 4\,\delta a_i^{(h)})\tau_i^2. \tag{7}$$

Here $\delta a_i^{(n)}$ and $\delta a_i^{(h)}$ are defined as

$$\delta a_i^{(n)} \equiv \langle a\rangle_i^{(n)} - \langle a\rangle_i,$$

$$\delta a_i^{(h)} \equiv \langle a\rangle_i^{(h)} - \langle a\rangle_i.$$

If interface values $a_i^{(n)}$ and $a_i^{(h)}$ in Eqs. (4), (5) are eliminated through Eqs. (6), (7), we will have a block-bidiagonal system of linear equations which can be solved for $\langle a\rangle_i^{(n)}$ and $\langle a\rangle_i^{(h)}$. If the set of resulting linear equations is exactly solved, it has been shown [15] that the resulting scheme is unconditionally stable for Courant numbers greater than unity. Through an analysis, it has been shown [15] that the shorter wavelength modes undergo the stronger damping, for a given wavelength the solution approaches the correct steady state in the limit of large Courant number, significant phase errors develop only for Courant numbers for which there is strong damping, and the scheme is able to compute a given wavelength mode at a considerably large Courant number without significant damping of the wave occurring.

Our purpose is to find an iterative approach for cell-averages $\langle a\rangle_i^{(n)}$ $(i = 1, 2, ...)$. From an initial guess for interface values $a_i^{(n)}$ and $a_i^{(h)}$, a straightforward procedure is to calculate cell-averages, $\langle a\rangle_i^{(n)}$ and $\langle a\rangle_i^{(h)}$, through Eqs. (4), (5) followed by an improvement of the interface values through Eqs. (6), (7). Unfortunately, numerical experiments show that this iterative procedure does not converge when the Courant number is larger than unity. This is because the error in $\langle a\rangle_i^{(n)}$ is increased by a factor of the Courant number through each iteration for Eq. (2).

Our approach for the linear advection is as follows. We eliminate $a_{i+1}^{(n)}$ and $a_{i+1}^{(h)}$ in Eqs. (4), (5) through Eqs. (6), (7) to obtain

$$(1 + \sigma_i\alpha_i^{(h)})\,\delta a_i^{(n)} + \sigma_i\beta_i^{(h)}\,\delta a_i^{(h)} = \sigma_i(a_i^{(h)} - \langle a\rangle_i), \tag{8}$$

$$\tfrac{1}{4}\sigma_i(3\alpha_i^{(h)} - \alpha_i^{(n)})\,\delta a_i^{(n)} + [1 + \tfrac{1}{4}\sigma_i(3\beta_i^{(h)} - \beta_i^{(n)})]\,\delta a_i^{(h)} = \tfrac{1}{4}\sigma_i(3a_i^{(h)} - a_i^{(n)}) - \tfrac{1}{2}\sigma_i\langle a\rangle_i. \tag{9}$$

Here $\alpha_i^{(n)}$, $\beta_i^{(n)}$, $\alpha_i^{(h)}$, and $\beta_i^{(h)}$ are defined as

$$\alpha_i^{(n)} \equiv \tau_i^{(h)}(2\tau_i^{(h)} - 1), \qquad \beta_i^{(n)} \equiv 4\tau_i^{(h)}(1 - \tau_i^{(h)}), \tag{10}$$

$$\alpha_i^{(h)} \equiv \tau_i(2\tau_i - 1), \qquad \beta_i^{(h)} \equiv 4\tau_i(1 - \tau_i). \tag{11}$$

We initially guess interface values, $a_i^{(n)}$ and $a_i^{(h)}$, and then calculate cell-averages $\langle a\rangle_i^{(n)}$ and $\langle a\rangle_i^{(h)}$ through solving Eqs. (8), (9) for $\delta a_i^{(n)}$ and $\delta a_i^{(h)}$. The interface values are improved through Eqs. (6), (7) with the right-hand side (RHS) of Eqs. (6), (7) evaluated at the improved cell-averages. One iteration consists of the two sets of calculations, one for Eqs. (8), (9) and the other for Eqs. (6), (7). The next iteration may be started from the improved interface values. Numerical experiments show that this iterative procedure converges. We will show the convergence later.

3. A SCHEME FOR HYPERBOLIC SYSTEMS OF CONSERVATION LAWS

Let us consider a hyperbolic system of conservation laws:

$$\frac{\partial \mathbf{U}}{\partial t} + \frac{\partial \mathbf{F}(\mathbf{U})}{\partial x} = 0. \tag{12}$$

Here $\mathbf{U}$ is a vector consisting of n variables $\mathbf{U} = (u_1, u_2, ..., u_n)^{\mathrm{T}}$, and $\mathbf{F}(\mathbf{U})$ is a flux vector $\mathbf{F}(\mathbf{U}) = (f_1(\mathbf{U}), f_2(\mathbf{U}), ..., f_n(\mathbf{U}))^{\mathrm{T}}$. The superscript T here stands for transpose. We define a matrix $\mathbf{A}(\mathbf{U})$ $(\equiv \{a_{jk}, j, k = 1, 2, ..., n\})$ by $a_{jk} \equiv \partial f_j(\mathbf{U})/\partial u_k$. Eigenvalues of the matrix $\mathbf{A}(\mathbf{U})$ denoted by c_k $(k = 1, 2, ..., n)$ are speeds of characteristic waves.

Suppose all wave speeds c_k are real. The system is strictly hyperbolic if all characteristic speeds c_k are distinct. Otherwise, it is nonstrictly hyperbolic. For example, the Euler equations form a strictly hyperbolic system with characteristic speeds $(u - c_s)$, u, and $(u + c_s)$. Here u and c_s are a flow velocity and a sound speed. Ideal MHD equations [25] form a nonstrictly hyperbolic system with characteristic speeds $(u - c_f)$, $(u - c_a)$, $(u - c_s)$, u, $(u + c_f)$, $(u + c_a)$, and $(u + c_s)$. Here c_f, c_a, and c_s are fast, Alfven, and slow wave speeds, and $c_f \geq c_a \geq c_s$. Both fast and slow waves are compressible, but Alfven waves are incompressible. When one or more components of a magnetic field vanish, wave speeds may become degenerate in ideal MHD equations.

We assume that an entropy wave (if it exists) has a vanishing wave speed, and each of the other wave speeds is either non-negative or non-positive. For many physical conservation laws, we may make a coordinate transformation and let a system to have the property. For example, the Euler equations and ideal MHD equations may be written in a Lagrangian coordinate, in which wave speeds of the Euler equations become $\pm C_s$ and 0 with C_s being a sound speed, and wave speeds of ideal MHD equations

are $\pm C_f$, $\pm C_a$, $\pm C_s$, and 0 with C_f, C_a, and C_s being the fast, Alfven, and slow wave speeds, respectively.

Considering a numerical grid $\{x_i\}$ and a time step Δt, and integrating Eq. (12) in a rectangular domain $x_i < x < x_{i+1}$ and $0 < t < \Delta t$, we obtain the following difference equation:

$$\langle \mathbf{U} \rangle_i^{(n)} = \langle \mathbf{U} \rangle_i - \frac{\Delta t}{\Delta x_i} (\overline{\mathbf{F}}_{i+1} - \overline{\mathbf{F}}_i). \tag{13}$$

Here Δx_i is the width of the cell $[x_i, x_{i+1}]$, $\langle \mathbf{U} \rangle_i^{(n)}$ (or $\mathbf{U}_i$) is a cell-average of $\mathbf{U}$ at $t = \Delta t$ (or $t = 0$) over the cell, and $\overline{\mathbf{F}}_i$ is a time-average of $\mathbf{F}$ over the time step. The cell-average and time-average are defined as

$$\langle \mathbf{U} \rangle_i^{(n)} \equiv \frac{1}{\Delta x_i} \int_{x_i}^{x_{i+1}} \mathbf{U}(x, \Delta t)\, dx,$$

$$\overline{\mathbf{F}}_i \equiv \frac{1}{\Delta t} \int_0^{\Delta t} \mathbf{F}[\mathbf{U}(x_i, t)]\, dt.$$

It should be noted that Eq. (13) is exact. In this paper, we will use an approximation

$$\overline{\mathbf{F}}(\mathbf{U}) = \mathbf{F}(\overline{\mathbf{U}}), \tag{14}$$

which is second-order accurate.

We approximately calculate a time-average through a linear interpolation of an interface value along time. The linear interpolation is uniquely determined by $\mathbf{U}_i^{(h)}$ and $\mathbf{U}_i^{(n)}$. Here $\mathbf{U}_i^{(h)} \equiv \mathbf{U}(x_i, \Delta t/2)$ and $\mathbf{U}_i^{(n)} \equiv \mathbf{U}(x_i, \Delta t)$. Therefore the difference Eq. (13) may be approximately written as

$$\langle \mathbf{U} \rangle_i^{(n)} = \langle \mathbf{U} \rangle_i - \frac{\Delta t}{\Delta x_i} [\mathbf{F}(\mathbf{U}_{i+1}^{(h)}) - \mathbf{F}(\mathbf{U}_i^{(h)})]. \tag{15}$$

Similarly, integrating Eq. (12) in a rectangular domain $x_i < x < x_{i+1}$ and $0 < t < \Delta t/2$, and using the linear interpolation, we have

$$\langle \mathbf{U} \rangle_i^{(h)} = \langle \mathbf{U} \rangle_i - \frac{\Delta t}{2\, \Delta x_i} [\mathbf{F}(\mathbf{U}_{i+1}^{(hn)}) - \mathbf{F}(\mathbf{U}_i^{(hn)})]. \tag{16}$$

Here

$$\mathbf{U}_i^{(hn)} \equiv \tfrac{3}{2}\mathbf{U}_i^{(h)} - \tfrac{1}{2}\mathbf{U}_i^{(n)}.$$

3.1. *Iterative Approach*

Our purpose in this subsection is to develop an iterative approach to find the interface value, $\mathbf{U}_i^{(h)}$, which is needed in Eq. (15). To this end, we first write Eq. (15) in a form:

$$\langle \mathbf{U} \rangle_i^{(n)} = \langle \mathbf{U} \rangle_i - \frac{\Delta t}{\Delta x_i} \mathbf{T}(\mathbf{U}_i^{(h)}, \mathbf{U}_{i+1}^{(h)})(\mathbf{U}_{i+1}^{(h)} - \mathbf{U}_i^{(h)}). \tag{17}$$

Here $\mathbf{T}(\mathbf{U}_i^{(h)}, \mathbf{U}_{i+1}^{(h)})(\mathbf{U}_{i+1}^{(h)} - \mathbf{U}_i^{(h)})$ comes from the Taylor expansion of the net flux $\Delta \mathbf{F} \equiv \mathbf{F}(\mathbf{U}_{i+1}^{(h)}) - \mathbf{F}(\mathbf{U}_i^{(h)})$. For example, suppose $\mathbf{F}(\mathbf{U})$ is a function of two variables, u and v. We write the net flux as

$$\begin{aligned}\Delta \mathbf{F} &= \mathbf{F}(u_{i+1}^{(h)}, v_{i+1}^{(h)}) - \mathbf{F}(u_i^{(h)}, v_{i+1}^{(h)}) \\ &\quad + \mathbf{F}(u_i^{(h)}, v_{i+1}^{(h)}) - \mathbf{F}(u_i^{(h)}, v_i^{(h)}) \\ &= \mathbf{T}_1(u_i^{(h)}, v_{i+1}^{(h)})(u_{i+1}^{(h)} - u_i^{(h)}) + \mathbf{T}_2(u_i^{(h)}, v_{i+1}^{(h)})(v_{i+1}^{(h)} - v_i^{(h)}) \\ &= (\mathbf{T}_1, \mathbf{T}_2)(\mathbf{U}_{i+1}^{(h)} - \mathbf{U}_i^{(h)}).\end{aligned}$$

Here $\mathbf{T}_1(u_i^{(h)}, v_{i+1}^{(h)})$ is the Taylor expansion of $[\mathbf{F}(u_{i+1}^{(h)}, v_{i+1}^{(h)}) - \mathbf{F}(u_i^{(h)}, v_{i+1}^{(h)})]$ at $(u_i^{(h)}, v_{i+1}^{(h)})$ divided by $(u_{i+1}^{(h)} - u_i^{(h)})$, and $\mathbf{T}_2(u_i^{(h)}, v_i^{(h)})$ is the Taylor expansion of $[\mathbf{F}(u_i^{(h)}, v_{i+1}^{(h)}) - \mathbf{F}(u_i^{(h)}, v_i^{(h)})]$ at $(u_i^{(h)}, v_i^{(h)})$ divided by $(v_{i+1}^{(h)} - v_i^{(h)})$. In this special case, $\mathbf{T}(\mathbf{U}_i^{(h)}, \mathbf{U}_{i+1}^{(h)}) = (\mathbf{T}_1, \mathbf{T}_2)$.

For a general $\mathbf{F}$ containing n variables, $u_1, u_2, ..., u_n$, we write the net flux as

$$\begin{aligned}\Delta \mathbf{F} = \sum_{k=1}^{k=n} [&\mathbf{F}(u_{1i+1}, u_{2i+1}, ..., u_{n-ki+1}, u_{n-k+1i}, ..., u_{ki}) \\ &- \mathbf{F}(u_{1i+1}, u_{2i+1}, ..., u_{n-k-1i+1}, u_{n-ki}, ..., u_{ki})],\end{aligned}$$

expand $\mathbf{F}(u_{1i+1}, u_{2i+1}, ..., u_{n-ki+1}, u_{n-k+1i}, ..., u_{ki}) - \mathbf{F}(u_{1i+1}, u_{2i+1}, ..., u_{n-k-1i+1}, u_{n-ki}, ..., u_{ki})$ at $(u_{1i+1}, u_{2i+1}, ..., u_{n-k-1i+1}, u_{n-ki}, ..., u_{ki})$ through the Taylor expansion, and then write the net flux $\Delta \mathbf{F}$ in the form $\mathbf{T}(\mathbf{U}_i^{(h)}, \mathbf{U}_{i+1}^{(h)})(\mathbf{U}_{i+1}^{(h)} - \mathbf{U}_i^{(h)})$.

Similarly, we write Eq. (16) as

$$\langle \mathbf{U} \rangle_i^{(h)} = \langle \mathbf{U} \rangle_i - \frac{\Delta t}{2\, \Delta x_i} \mathbf{T}(\mathbf{U}_i^{(hn)}, \mathbf{U}_{i+1}^{(hn)})(\mathbf{U}_{i+1}^{(hn)} - \mathbf{U}_i^{(hn)}). \tag{18}$$

Thus, we have written cell-averages in terms of interface values in Eqs. (17), (18) which are equivalent to Eqs. (4), (5) for the linear advection.

On the other hand, we have to write interface values, $\mathbf{U}_{i+1}^{(h)}$ and $\mathbf{U}_{i+1}^{(n)}$, in terms of cell-averages. To this end, we use a Riemann solver [26] for hyperbolic systems of conservation laws. Following a standard procedure [27], we may obtain differentials of Riemann invariants for n characteristic waves:

$$dR_k = \mathbf{L}_k^T(\mathbf{U})\, d\mathbf{U} \qquad \text{for } k = 1, 2, ..., n. \tag{19}$$

Here $\mathbf{L}_k(\mathbf{U})$ is the left eigenvector of $\mathbf{A}(\mathbf{U})$ associated with the kth characteristic wave c_k. Along the characteristic curve determined by $dx = c_k(\mathbf{U})\, dt$, $dR_k = 0$.

In order to find the interface value $\mathbf{U}_{i+1}^{(h)}$, we trace all

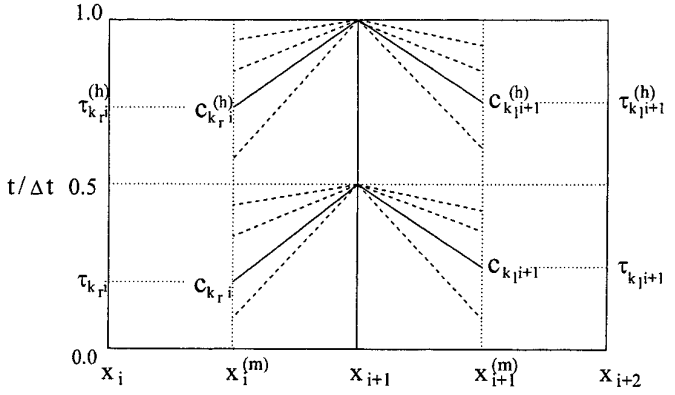

FIG. 2. An illustration for calculation of interface values at $x = x_{i+1}$ and $t = \Delta t/2$ and $t = \Delta t$ in the case with Courant numbers associated with all waves larger than unity. Two sets of characteristics are traced back to the centers of two neighbor cells, $x_i^{(m)}$ and $x_{i+1}^{(m)}$. Interface values at x_{i+1} and at $t = \Delta t/2$ and Δt may be obtained through solving two Riemann problems, and may be written in terms of cell-averages at various time levels. A cell-average at $t \in [0, \Delta t]$ may be approximately calculated through a parabolic interpolation in time, and the parabola is uniquely determined by cell-averages at $t = 0$, $\Delta t/2$, and Δt.

the characteristic curves passing through the point $(x_{i+1}, \Delta t/2)$ back to centers of two neighbor cells, $x_i^{(m)}$ and $x_{i+1}^{(m)}$ (see Fig. 2). Time levels at the ends of the characteristic curves at the center $x_i^{(m)}$ are $\tau_{k_r i}\,\Delta t$. Here k_r may be any wave propagating to the right. Time levels at the ends of the characteristic curves at the center $x_{i+1}^{(m)}$ are $\tau_{k_l i+1}\,\Delta t$. Here k_l may be any wave propagating to the left. $\tau_{k_r i}$ and $\tau_{k_l i}$ are uniformly defined as

$$\tau_{ki} \equiv \frac{1}{2}\left(1 - \frac{\Delta x_i}{c_{ki}\,\Delta t}\right). \tag{20}$$

Here c_{ki} is the wave speed c_k evaluated at $\mathbf{U}_i$. The interface value $\mathbf{U}_{i+1}^{(h)}$ may be found through a Riemann problem, in which the left state associated with the k_rth wave is $\mathbf{U}(x_i, \tau_{k_r i}\,\Delta t)$, and the right state associated with the k_lth wave is $\mathbf{U}(x_{i+1}, \tau_{k_l i+1}\,\Delta t)$. Therefore, $\mathbf{U}_{i+1}^{(h)}$ may be obtained through a set of linear equations:

$$\bar{\mathbf{L}}_k(\mathbf{U}_i, \mathbf{U}_{i+1})[\mathbf{U}_{i+1}^{(h)} - \mathbf{U}(x_i^{(m)}, \tau_{ki}\,\Delta t)] = 0 \qquad \text{for } c_k > 0, \tag{21}$$

$$\bar{\mathbf{L}}_k(\mathbf{U}_i, \mathbf{U}_{i+1})[\mathbf{U}_{i+1}^{(h)} - \mathbf{U}(x_{i+1}^{(m)}, \tau_{ki+1}\,\Delta t)] = 0 \qquad \text{for } c_k < 0, \tag{22}$$

$$\bar{\mathbf{L}}_k(\mathbf{U}_i, \mathbf{U}_{i+1})[\mathbf{U}_{i+1}^{(h)} - \mathbf{U}(x_{i+1}, 0)] = 0 \qquad \text{for } c_k = 0. \tag{23}$$

Here

$$\bar{\mathbf{L}}_k(\mathbf{U}_i, \mathbf{U}_{i+1}) \equiv \tfrac{1}{2}\,\text{sign}\{\mathbf{D}[\mathbf{L}_k(\mathbf{U}_i)]\}\{\text{abs}[\mathbf{L}_k(\mathbf{U}_i)] + \text{abs}[\mathbf{L}_k(\mathbf{U}_{i+1})]\} \qquad \text{for } c_k > 0,$$

$$\bar{\mathbf{L}}_k(\mathbf{U}_i, \mathbf{U}_{i+1}) \equiv \tfrac{1}{2}\,\text{sign}\{\mathbf{D}[\mathbf{L}_k(\mathbf{U}_{i+1})]\}\{\text{abs}[\mathbf{L}_k(\mathbf{U}_i)] + \text{abs}[\mathbf{L}_k(\mathbf{U}_{i+1})]\} \qquad \text{for } c_k < 0,$$

$$\bar{\mathbf{L}}_k(\mathbf{U}_i, \mathbf{U}_{i+1}) \equiv \tfrac{1}{2}\{\mathbf{L}_k(\mathbf{U}_i) + \mathbf{L}_k(\mathbf{U}_{i+1})\} \qquad \text{for } c_k = 0.$$

$\mathbf{D}(\mathbf{L})$ ($\equiv\{d_{ij},\ i, j = 1, 2, ..., n\}$) is defined as a diagonal matrix with d_{jj} equal to the jth element of the vector $\mathbf{L}$, sign($\mathbf{D}$) is defined as a diagonal matrix whose elements are signs of elements of $\mathbf{D}$, and abs($\mathbf{L}$) is defined as a vector whose elements are absolute values of elements of the vector $\mathbf{L}$.

Similarly, the interface value $\mathbf{U}_{i+1}^{(n)}$ may be found through another set of linear equations:

$$\bar{\mathbf{L}}_k(\langle\mathbf{U}\rangle_i^{(h)}, \langle\mathbf{U}\rangle_{i+1}^{(h)})[\mathbf{U}_{i+1}^{(n)} - \mathbf{U}(x_i^{(m)}, \tau_{ki}^{(h)}\,\Delta t)] = 0 \qquad \text{for } c_k > 0, \tag{24}$$

$$\bar{\mathbf{L}}_k(\langle\mathbf{U}\rangle_i^{(h)}, \langle\mathbf{U}\rangle_{i+1}^{(h)})[\mathbf{U}_{i+1}^{(n)} - \mathbf{U}(x_{i+1}^{(m)}, \tau_{ki+1}^{(h)}\,\Delta t)] = 0 \qquad \text{for } c_k < 0, \tag{25}$$

$$\bar{\mathbf{L}}_k(\langle\mathbf{U}\rangle_i^{(h)}, \langle\mathbf{U}\rangle_{i+1}^{(h)})[\mathbf{U}_{i+1}^{(n)} - \mathbf{U}(x_{i+1}, 0)] = 0. \tag{26}$$

Here

$$\tau_{ki}^{(h)} = 1 - \frac{\Delta x_i}{2c_{ki}^{(h)}\,\Delta t},$$

and $c_{ki}^{(h)}$ is the wave speed c_k evaluated at $\langle\mathbf{U}\rangle_i^{(h)}$.

Up to second order of accuracy, $\mathbf{U}(x_i^{(m)}, t)$ is equal to a cell-average of $\mathbf{U}$ at the time t. A cell-average at any time $t \in [0, \Delta t]$ may be found through a parabolic interpolation in time. The parabola is uniquely determined by $\langle\mathbf{U}\rangle_i$, $\langle\mathbf{U}\rangle_i^{(h)}$, and $\langle\mathbf{U}\rangle_i^{(n)}$. Thus $\mathbf{U}(x_i^{(m)}, \tau_{ki}\,\Delta t)$, $\mathbf{U}(x_{i+1}^{(m)}, \tau_{ki+1}\,\Delta t)$, $\mathbf{U}(x_i^{(m)}, \tau_{ki}^{(h)}\,\Delta t)$, and $\mathbf{U}(x_{i+1}^{(m)}, \tau_{ki+1}^{(h)}\,\Delta t)$ in Eqs. (21), (22), (24), (25) may be written in terms of $\langle\mathbf{U}\rangle_i$, $\langle\mathbf{U}\rangle_i^{(h)}$, and $\langle\mathbf{U}\rangle_i^{(n)}$:

$$\mathbf{U}(x_i^{(m)}, \tau_i\,\Delta t) = \langle\mathbf{U}\rangle_i + (-\delta\mathbf{U}_i^{(n)} + 4\,\delta\mathbf{U}_i^{(h)})\tau_i + (2\,\delta\mathbf{U}_i^{(n)} - 4\,\delta\mathbf{U}_i^{(h)})\tau_i^2. \tag{27}$$

Here τ_i may be either τ_{ki} or $\tau_{ki}^{(h)}$, and

$$\delta\mathbf{U}_i^{(n)} \equiv \langle\mathbf{U}\rangle_i^{(n)} - \langle\mathbf{U}\rangle_i, \qquad \delta\mathbf{U}_i^{(h)} \equiv \langle\mathbf{U}\rangle_i^{(h)} - \langle\mathbf{U}\rangle_i.$$

Solving Eqs. (21)–(23) for $\mathbf{U}_{i+1}^{(h)}$ and using Eq. (27), we obtain

$$\mathbf{U}_{i+1}^{(h)} = \mathbf{U}_{i+1}^{(h0)} + \mathbf{H}_{i+1}^{(n)}\,\delta\mathbf{U}_i^{(n)} + \mathbf{H}_{i+1}^{(h)}\,\delta\mathbf{U}_i^{(h)} + \mathbf{H}_{i+1}^{(np)}\,\delta\mathbf{U}_{i+1}^{(n)} + \mathbf{H}_{i+1}^{(hp)}\,\delta\mathbf{U}_{i+1}^{(h)}. \tag{28}$$

Here the vector $\mathbf{U}_{i+1}^{(h0)}$ and matrices $\mathbf{H}_{i+1}^{(n)}, \mathbf{H}_{i+1}^{(h)}, \mathbf{H}_{i+1}^{(np)}$, and $\mathbf{H}_{i+1}^{(np)}$ depend on only initial values $\mathbf{U}_i$ and τ_{ki}. Similarly, solving Eqs. (24)–(26) for $\mathbf{U}_{i+1}^{(n)}$ and using Eq. (27), we have

$$\mathbf{U}_{i+1}^{(n)} = \mathbf{U}_{i+1}^{(n0)} + \mathbf{N}_{i+1}^{(n)}\,\delta\mathbf{U}_i^{(n)} + \mathbf{N}_{i+1}^{(h)}\,\delta\mathbf{U}_i^{(h)} + \mathbf{N}_{i+1}^{(np)}\,\delta\mathbf{U}_{i+1}^{(n)} + \mathbf{N}_{i+1}^{(hp)}\,\delta\mathbf{U}_{i+1}^{(h)}. \tag{29}$$

The vector $\mathbf{U}_{i+1}^{(n0)}$ and matrices $N_{i+1}^{(n)}, \mathbf{N}_{i+1}^{(h)}, \mathbf{N}_{i+1}^{(np)}$, and $\mathbf{N}_{i+1}^{(hp)}$ have the same forms as those used in Eq. (28) if we make the following substitutions:

$$\langle\mathbf{U}\rangle_i^{(h)} \to \langle\mathbf{U}\rangle_i, \qquad \tau_{ki}^{(h)} \to \tau_{ki}, \qquad \Delta t \to \Delta t/2.$$

In order to find an iterative approach for interface values which are needed in the Godunov scheme Eq. (15), we substitute Eq. (28) into Eq. (17) for $\mathbf{U}_{i+1}^{(h)}$ and $\mathbf{U}_i^{(h)}$. It should be noted that $\mathbf{T}(\mathbf{U}_i^{(h)}, \mathbf{U}_{i+1}^{(h)})$ in Eq. (17) is left alone when we do the substitution. We may write the result in the form:

$$[\mathbf{I} + \mathbf{Q}_i^{(n)}]\,\delta\mathbf{U}_i^{(n)} + \mathbf{R}_i^{(n)}\,\delta\mathbf{U}_i^{(h)} = \mathbf{S}_i^{(n)}. \tag{30}$$

Here $\mathbf{I}$ is a unity matrix, and matrices $\mathbf{Q}_i^{(n)}$, $\mathbf{R}_i^{(n)}$, and vector $\mathbf{S}_i^{(n)}$ are defined as

$$\mathbf{Q}_i^{(n)} \equiv \frac{\Delta t}{\Delta x_i}\mathbf{T}_i^{(h)}[\mathbf{H}_{i+1}^{(n)} - \mathbf{H}_i^{(np)}],$$

$$\mathbf{R}_i^{(n)} \equiv \frac{\Delta t}{\Delta x_i}\mathbf{T}_i^{(h)}[\mathbf{H}_{i+1}^{(h)} - \mathbf{H}_i^{(hp)}],$$

$$\mathbf{S}_i^{(n)} \equiv -\frac{\Delta t}{\Delta x_i}\mathbf{T}_i^{(h)}[\mathbf{U}_{i+1}^{(h0)} - \mathbf{U}_i^{(h0)} + \mathbf{H}_{i+1}^{(np)}\,\delta\mathbf{U}_{i+1}^{(n)} + \mathbf{H}_{i+1}^{(hp)}\,\delta\mathbf{U}_{i+1}^{(h)} - \mathbf{H}_i^{(n)}\,\delta\mathbf{U}_{i-1}^{(n)} - \mathbf{H}_i^{(h)}\,\delta\mathbf{U}_{i-1}^{(h)}],$$

$$\mathbf{T}_i^{(h)} \equiv \mathbf{T}(\mathbf{U}_i^{(h)}, \mathbf{U}_{i+1}^{(h)}).$$

Similarly, substituting Eqs. (29) into Eq. (18) for $\mathbf{U}_{i+1}^{(h)}, \mathbf{U}_{i+1}^{(n)}, \mathbf{U}_i^{(h)}$, and $\mathbf{U}_i^{(n)}$, and leaving $\mathbf{T}(\mathbf{U}_i^{(hn)}, \mathbf{U}_{i+1}^{(hn)})$ alone, we may write Eq. (18) as

$$\mathbf{Q}_i^{(h)}\,\delta\mathbf{U}_i^{(n)} + [\mathbf{I} + \mathbf{R}_i^{(h)}]\,\delta\mathbf{U}_i^{(h)} = \mathbf{S}_i^{(h)}. \tag{31}$$

Here matrices $\mathbf{Q}_i^{(h)}, \mathbf{R}_i^{(h)}$, and vector $\mathbf{S}_i^{(h)}$ are defined as

$$\mathbf{Q}_i^{(h)} \equiv \frac{\Delta t}{2\,\Delta x_i}\mathbf{T}_i^{(hn)}[\mathbf{M}_{i+1}^{(n)} - \mathbf{M}_i^{(np)}],$$

$$\mathbf{R}_i^{(h)} \equiv \frac{\Delta t}{2\,\Delta x_i}\mathbf{T}_i^{(hn)}[\mathbf{M}_{i+1}^{(h)} - \mathbf{M}_i^{(hp)}],$$

$$\mathbf{S}_i^{(h)} \equiv -\frac{\Delta t}{2\,\Delta x_i}\mathbf{T}_i^{(hn)}[\mathbf{U}_{i+1}^{(hn0)} - \mathbf{U}_i^{(hn0)} + \mathbf{M}_{i+1}^{(np)}\,\delta\mathbf{U}_{i+1}^{(n)} + \mathbf{M}_{i+1}^{(hp)}\,\delta\mathbf{U}_{i+1}^{(h)} - \mathbf{M}_i^{(n)}\,\delta\mathbf{U}_{i-1}^{(n)} - \mathbf{M}_i^{(h)}\,\delta\mathbf{U}_{i-1}^{(h)}],$$

$$\mathbf{T}_i^{(hn)} \equiv \mathbf{T}(\mathbf{U}_i^{(hn)}, \mathbf{U}_{i+1}^{(hn)}),$$

$$\mathbf{U}_i^{(hn0)} \equiv \tfrac{3}{2}\mathbf{U}_i^{(h0)} - \tfrac{1}{2}\mathbf{U}_i^{(n0)},$$

$$\mathbf{M}_i^{(n)} \equiv \tfrac{3}{2}\mathbf{H}_i^{(n)} - \tfrac{1}{2}\mathbf{N}_i^{(n)}, \qquad \mathbf{M}_i^{(np)} \equiv \tfrac{3}{2}\mathbf{H}_i^{(np)} - \tfrac{1}{2}\mathbf{N}_i^{(np)},$$

$$\mathbf{M}_i^{(h)} \equiv \tfrac{3}{2}\mathbf{H}_i^{(h)} - \tfrac{1}{2}\mathbf{N}_i^{(h)}, \qquad \mathbf{M}_i^{(hp)} \equiv \tfrac{3}{2}\mathbf{H}_i^{(hp)} - \tfrac{1}{2}\mathbf{N}_i^{(hp)}.$$

One iterative procedure for interface values is as follows. Initially, we guess $\langle\mathbf{U}\rangle_i^{(n)}$, $\langle\mathbf{U}\rangle_i^{(h)}$, $\mathbf{U}_i^{(n)}$, and $\mathbf{U}_i^{(h)}$. We improve $\langle\mathbf{U}\rangle_i^{(n)}$ and $\langle\mathbf{U}\rangle_i^{(h)}$ through solving Eqs. (30), (31) for $\delta\mathbf{U}_i^{(n)}$ and $\delta\mathbf{U}_i^{(h)}$. Thus we are solving a set of linear equations with coefficients evaluated at the values obtained from the last iteration. Then we substitute the improved $\langle\mathbf{U}\rangle_i^{(n)}$ and $\langle\mathbf{U}\rangle_i^{(h)}$ into the RHS of Eqs. (17, 18) and improve $\mathbf{U}_i^{(n)}$ and $\mathbf{U}_i^{(h)}$. One iteration consists of the two sets of calculations, one for Eqs. (30), (31) and the other for Eqs. (17), (18). The next iteration may be started with the improved cell-averages and interface values if necessary. Numerical experiments for the advection, the Euler equations, and ideal MHD equations show that this iterative procedure converges. We call the approach $\mathbf{A}_1$.

For the calculation of interface values in this implicit–explicit hybrid scheme, each wave may be either implicitly or explicitly treated depending on the Courant number associated with the wave in each cell. For example, if $c_{ki}\,\Delta t/\Delta x_i$ is less than unity, then $\mathbf{U}(x_i^{(m)}, \tau_{ki}\,\Delta t)$ in Eq. (21) should be explicitly calculated from a domain-average for the kth wave, and all other characteristic fields are implicitly treated if their associated Courant numbers are larger than unity.

3.2. *Multi-colors and Convergence of Iterations*

Now we discuss the speed of convergence. The convergence is closely related to the propagation of information in each iteration. Information travels only one numerical cell during each iteration in the primitive approach $\mathbf{A}_1$. In order to improve the speed of convergence, we divide numerical cells into two sets: $\{i;\, i = 2j + 1,\, j = 0, 1, 2, \ldots\}$ and $\{i;\, i = 2j,\, j = 1, 2, \ldots\}$, which are called red and black sets. Equations (30), (31) are first implemented for the red set of cells, followed by the implementation for the other set of cells. We call this approach $\mathbf{A}_2$, which results in a faster convergence than $\mathbf{A}_1$ since information travels two cells during each iteration.

To further develop the red/black strategy, we divide all

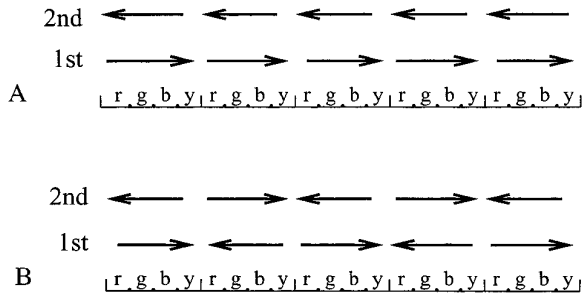

FIG. 3. An illustration for $\mathbf{A}_4$ (A) and $\mathbf{B}_4$ (B). Twenty cells are divided into five bins, each of which contains four cells labeled as r(ed), g(reen), b(lue), and y(ellow). The order to implement Eqs. (30), (31) for cells with different colors in each bin are shown by the arrows in the first and second iterations.

numerical cells into k groups, i.e., k colors: $\mathbf{G}_l$ ($l = 1, 2, ..., k$), and the lth group contains cells $\{i; i = (j-1)k + l, j = 1, 2, ...\}$. An iteration consists of the implementation of Eqs. (30), (31) consecutively for groups $\mathbf{G}_1, \mathbf{G}_2, ..., \mathbf{G}_k$ followed by another iteration with the opposite order, i.e., from $\mathbf{G}_k$ consecutively to $\mathbf{G}_1$. We call the approach $\mathbf{A}_k$. The approach $\mathbf{A}_k$ is illustrated in Fig. 3A where all numerical cells are divided into five bins, and four cells in each bin are labeled as r(ed), g(reen), b(lue), and y(ellow). In the first iteration, Eqs. (30), (31) are consecutively implemented for all red cells, all green cells, all blue cells, and all yellow cells. In the second iteration, the order in each bin is opposite to that in the first iteration. The arrows in Fig. 3A indicate the orders of the implementation for different colors in each bin during the first and second iterations. Information may travel k cells in the approach $\mathbf{A}_k$.

Although information may travel k cells during one iteration, it is not true for the cells in different bins in Fig. 3A. The approach $\mathbf{B}_k$ illustrated in Fig. 3B makes a further improvement for convergence. As illustrated in Fig. 4B, during the first iteration, Eqs. (30), (31) are first implemented for the red cells in the 1st, 3rd, and 5th bins, and for the yellow cells in the 2nd and 4th bins; then are implemented for the green cells in the 1st, 3rd, and 5th bins and for the blue cells in the 2nd and 4th bins; after that, they are implemented for the blue cells in the 1st, 3rd, and 5th bins and for the green cells in the 2nd and 4th bins; and as the final step in the first iteration, they are implemented for the yellow cells in the 1st, 3rd, and 5th bins and for the red cells in the 2nd and 4th bins. In the second iteration, the order of the implementation for different colors in each bin is opposite to that in the last iteration. The arrows in Fig. 4B show the orders of the implementation for different colors in each bin during the first and second iterations.

We mention two points for the iterative approach. First, coefficients in Eqs. (30), (31) are evaluated only once in each iteration in both $\mathbf{A}_k$ and $\mathbf{B}_k$, and thus use of multicolors does not involve more calculations than a single color. Second, for the flux calculation needed in scheme Eq. (15), we do not have to find converged interface values. Only approximate interface values are needed.

As the final part of this subsection, we address the nonstrict hyperbolicity. For a system losing the strict hyperbolicity, eigenvalues $c_k(\mathbf{U})$ ($k = 1, 2, ..., n$) may become degenerate at some state $\mathbf{U}^*$. Mathematically, the degeneracy may cause a singularity when Eqs. (21)–(23) are solved. To physically remove the degeneracy requires a more complete set of equations than the conservation laws themselves. We use the same approach as that in [26] to remove the degeneracy. If the eigenvalues become degenerate at $\mathbf{U}^*$, we replace the local $\mathbf{U}$ by $(\mathbf{U}^* + \delta)$ when solving Eqs. (21)–(23). Here δ is a vector with small values for its elements. δ should be sufficiently small but within the accuracy of digits of an actual machine. The influence of the artificial δ on numerical results is negligible if δ is very small. Actual values of δ may depend on specific conservation laws.

4. NUMERICAL EXAMPLES

The feature of the implicit–explicit hybrid scheme presented in the last section will be shown here for the Euler equations and ideal MHD equations. In this paper, we limit the discussion to the γ-law for the equation of state, although a more general equation of state may be accommodated. The dynamical step for these two sets of equations will be carried out in a Lagrangian grid followed by an explicit mapping [26] from Lagrangian to Eulerian grids.

4.1. *The One-Dimensional Euler Equations*

The one-dimensional Euler equations are

$$\frac{\partial \rho}{\partial t} + \frac{\partial}{\partial x}(\rho u) = 0,$$

$$\frac{\partial}{\partial t}(\rho u) + \frac{\partial}{\partial x}(\rho u^2 + p) = 0,$$

$$\frac{\partial}{\partial t}(\rho E) + \frac{\partial}{\partial x}[u(\rho E + p)] = 0.$$

Here ρ is the mass density, u is the flow velocity, p is the pressure, and E is the total specific energy defined by $E \equiv e + \rho u^2/2$ with e being the specific internal energy. The pressure is related to the internal energy density through the γ-law $p = (\gamma - 1)\rho e$ with γ being the ratio of specific heat capacities. The equations may be written in a Lagrangian form:

$$\frac{\partial V}{\partial t} = \frac{\partial u}{\partial m}, \tag{32}$$

$$\frac{\partial u}{\partial t} = -\frac{\partial p}{\partial m}, \tag{33}$$

$$\frac{\partial E}{\partial t} = -\frac{\partial uP}{\partial m}, \tag{34}$$

where V is the specific volume ($\equiv 1/\rho$), and m is the mass coordinate defined by $dm \equiv \rho\, dx$. Differentials of Riemann invariants for two sound waves in Eqs. (32)–(34) are

$$dR_{\pm} \equiv dp \pm C_s\, du. \tag{35}$$

Here the plus (or minus) sign is for the wave propagating in the positive (or negative) x-direction, and C_s is a sound speed in the mass coordinate, $C_s \equiv (\gamma\rho p)^{1/2}$. The sound speed in the x-coordinate, c_s, may be obtained through C_s divided by ρ. The simulation domain is one wavelength L ($= 1$). The initial wave is set up through differentials of Riemann invariants:

$$\frac{dR_+}{dx} = 0.4 \sin(2\pi x), \tag{36}$$

$$\frac{dR_-}{dx} = \frac{dR_0}{dx} = 0, \tag{37}$$

and $\rho(0, 0) = \rho_0$ ($= \gamma = \frac{5}{3}$) and $p(0, 0) = p_0$ ($\equiv 1$). Here $R_0 \equiv pV^{\gamma}$. We measure the convergence by the difference between the converged solution and the solution from each iteration:

$$\varepsilon_{1d} = \frac{1}{L}\sum_{i=1}^{N} \Delta x_i^{(n)} \left[\frac{1}{p_0}\left|p_i^{(n)} - p_{i,*}^{(n)}\right| + \frac{1}{c_0}\left|u_i^{(n)} - u_{i,*}^{(n)}\right|\right] + \frac{1}{L}\sum_{i=1}^{N} \Delta x_i^{(h)} \left[\frac{1}{p_0}\left|p_i^{(h)} - p_{i,*}^{(h)}\right| + \frac{1}{c_0}\left|u_i^{(h)} - u_{i,*}^{(h)}\right|\right]. \tag{38}$$

Here the subscript $*$ stands for the converged solution, and $\Delta x_i^{(n)}$ and $\Delta x_i^{(h)}$ are the widths of the ith cell in the Lagrangian coordinate at $t = \Delta t$ and $\Delta t/2$. The dotted line in Fig. 4 shows the relation between ε_{1d} and the number of iterations obtained from $\mathbf{A}_1$ when a uniform grid with N ($= 256$) numerical cells are used in [0, 1], and $\Delta t = 0.195313$. The Courant numbers, $c_s\, \Delta t/\Delta x$, are around 50. Dashed lines in Fig. 4 show the convergence of the approach $\mathbf{A}_k$ for $k = 2$, 8, 32, 64, and 128, and solid lines show the convergence of the approach $\mathbf{B}_k$ for the same initial condition and time step.

The first numerical example is the propagation of a sound wave initially given by Eqs. (36), (37) with a shifted flow velocity u_x. The initial condition is shown by the dotted lines in Fig. 5. The time step is 0.005. At each time step, each characteristic field is partially implicitly and partially explicitly calculated. Solid lines in Fig. 5 are the profiles at $t = 0.5$, 1.0, 1.5, and 2.0. This example shows a smooth switch between explicit and implicit calculations.

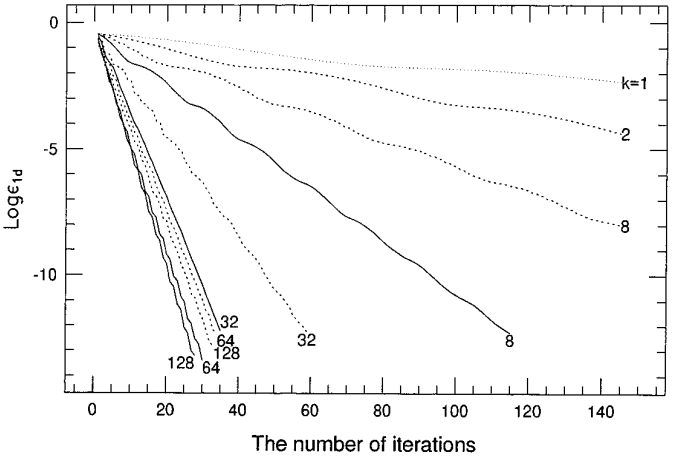

FIG. 4. The convergence obtained for the Euler equations: 256 cells in [0, 1], $\Delta t = 0.195$. Courant numbers are around 50. The wave travels about one-fifth of its wavelength during the time step. The dotted lines indicated by $k = 1$ results from the approach $\mathbf{A}_1$, the dashed lines are obtained from the approach $\mathbf{A}_k$ for $k = 2$, 8, 32, 64, and 128, and the solid lines are obtained from the approach $\mathbf{B}_k$ for $k = 8$, 32, 64, and 128.

Figure 6 shows the profiles (solid lines) of the wave after one time step when different time steps are used. The dotted lines in the figure are initial profiles, and dashed lines, which are considered as references, are obtained from the piecewise parabolic method [6]. When $c_s\, \Delta t/\Delta x \approx 20$, it is hard to see the difference between the implicit and explicit schemes.

4.2. *Ideal Magnetohydrodynamical Equations*

Effort has been paid for MHD calculations without or partially without time step restrictions [28–38]. One approach is to make use of reduced MHD equations [28, 29] or incompressible models [30, 32] which eliminate fast waves. In another typical approach for MHD calculations, artificial terms are added to time-discretized equations to provide means of stability [34–38]. In this subsection, we will illustrate the feature of the scheme described in the third section through simulations for ideal MHD equations. One-dimensional ideal MHD equations [25] are

$$\frac{\partial \rho}{\partial t} + \frac{\partial}{\partial x}(\rho u_x) = 0,$$

$$\frac{\partial}{\partial t}(\rho u_x) + \frac{\partial}{\partial x}(\rho u_x^2 + P) = 0,$$

$$\frac{\partial}{\partial t}(\rho u_y) + \frac{\partial}{\partial x}(\rho u_x u_y + P_y) = 0,$$

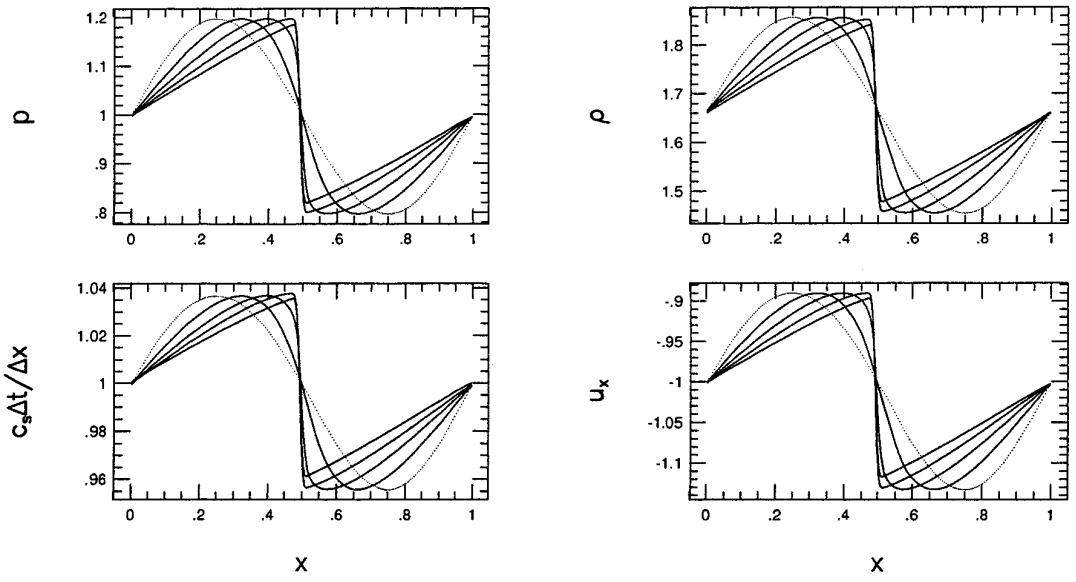

FIG. 5. The propagation of a sound wave, with 200 cells in [0, 1], $\Delta t = 0.005$, and 2 iterations. The dotted lines are initial profiles, the solid lines are the profiles at $t = 0.5$, 1.0, 1.5, and 2.0. The results show a smooth switch between explicit and implicit calculations.

$$\frac{\partial}{\partial t}(\rho u_z) + \frac{\partial}{\partial x}(\rho u_x u_z + P_z) = 0,$$

$$\frac{\partial}{\partial t}(\rho E) + \frac{\partial}{\partial x}(\rho u_x E + u_x P + u_y P_y + u_z P_z) = 0,$$

$$\frac{\partial B_y}{\partial t} - \frac{\partial}{\partial x}(u_y B_x - u_x B_y) = 0,$$

$$\frac{\partial B_z}{\partial t} - \frac{\partial}{\partial x}(u_z B_x - u_x B_z) = 0.$$

Here ρ is the mass density, and (u_x, u_y, u_z) and (B_x, B_y, B_z) are three components of the flow velocity and magnetic field, respectively. B_x is a constant under the one-dimensional approximation. E is the specific total energy, and P, P_y, and P_z are diagonal and off-diagonal total pressures. E, P, P_y, and P_z are defined as

$$E \equiv e + \frac{1}{2}(u_x^2 + u_y^2 + u_z^2) + \frac{1}{8\pi\rho}(B_x^2 + B_y^2 + B_z^2),$$

$$P \equiv p + \frac{1}{8\pi}(B_y^2 + B_z^2 - B_x^2),$$

$$P_y \equiv -\frac{1}{4\pi} B_x B_y, \qquad P_z \equiv -\frac{1}{4\pi} B_x B_z.$$

Here e is the specific internal energy and p is the thermal pressure.

Again, we will implement the dynamical step in a Lagrangian coordinate followed by an explicit mapping at the end of each dynamical step. Therefore we write the equations in a Lagrangian form:

$$\frac{\partial \mathbf{U}}{\partial t} + \frac{\partial \mathbf{F}(\mathbf{U})}{\partial m} = 0, \tag{39}$$

$$\mathbf{U} \equiv \begin{pmatrix} V \\ u_x \\ u_y \\ u_z \\ VB_y \\ VB_z \\ E \end{pmatrix}, \qquad \mathbf{F}(\mathbf{U}) \equiv \begin{pmatrix} -u_x \\ P \\ P_y \\ P_z \\ -B_x u_y \\ -B_x u_z \\ Pu_x + P_y u_y + P_z u_z \end{pmatrix}.$$

Here $V \equiv 1/\rho$, and m is a mass coordinate defined by $dm \equiv \rho\, dx$.

Differentials of Riemann invariants for two fast waves, two slow waves, and two Alfven waves respectively have forms:

$$dR_{f\pm} = (C_f^2 - C_a^2)(dP \pm C_f\, du_x) + \rho P_y (dP_y \pm C_f\, du_y) + \rho P_z (dP_z \pm C_f\, du_z), \tag{40}$$

$$dR_{s\pm} = (C_s^2 - C_a^2)(dP \pm C_s\, du_x) + \rho P_y (dP_y \pm C_s\, du_y) + \rho P_z (dP_z \pm C_s\, du_z), \tag{41}$$

$$dR_{a\pm} = \pm C_a (B_z\, du_y - B_y\, du_z) + (B_z\, dP_y - B_y\, dP_z). \tag{42}$$

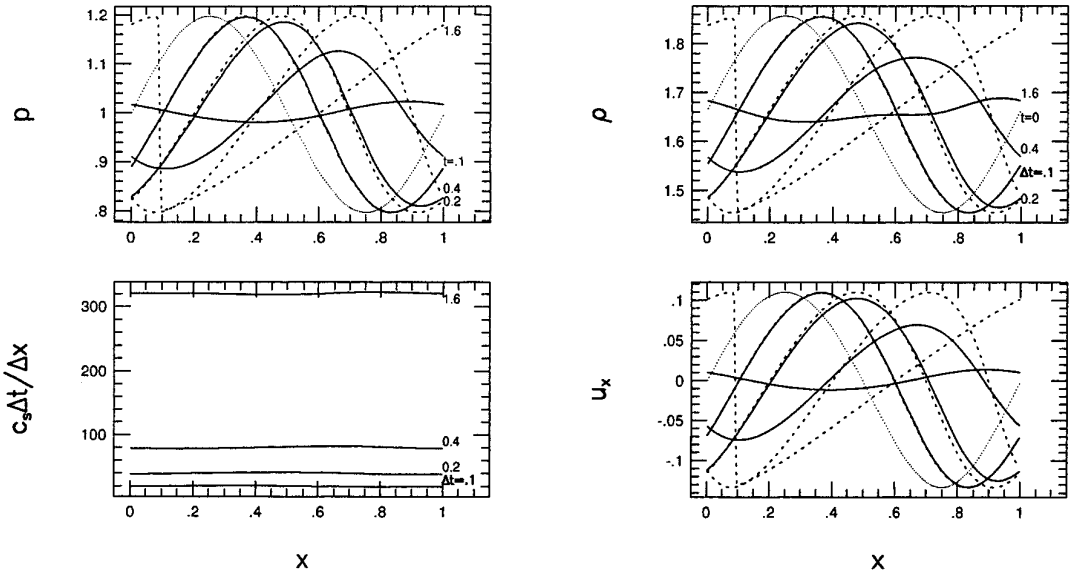

FIG. 6. A sound wave (solid lines) after one time step when different time steps are used, with 200 cells in [0, 1] and $\mathbf{B}_{25}$. Dotted lines are the initial condition, and the dashed lines are references obtained from an explicit scheme. Six iterations are used for $\Delta t = 0.1$; 10 iterations for $\Delta t = 0.2$; 14 iterations for $\Delta t = 0.4$; and 40 iterations for $\Delta t = 1.6$.

Here the plus (or minus) sign is for a wave propagating to the positive (or negative) x-direction. C_a, C_f, and C_s are the wave speeds for Alfven, fast, and slow waves in the mass coordinate respectively, and they are

$$C_a = \sqrt{\rho B_x^2/4\pi},$$

$$C_{f,s} = \frac{1}{\sqrt{2}}\{C_0^2 + C_a^2 + C_t^2 \pm \sqrt{(C_0^2 + C_a^2 + C_t^2)^2 - 4C_0^2C_a^2}\}^{1/2}.$$

Here the plus (or minus) sign is for the fast (or slow) wave speed, and C_0^2 and C_t^2 are defined as $C_0^2 \equiv \gamma p\rho$ and $C_t^2 \equiv \rho(B_y^2 + B_z^2)/4\pi$. Wave speeds in the x-coordinate, c_a, c_f, and c_s, may be obtained through C_a, C_f, and C_s divided by the mass density ρ.

We choose a nonlinear slow wave as an example. The initial wave with unity wavelength ($L = 1$) is set up through differentials of Riemann invariants:

$$\frac{dR_{s+}}{dx} = -0.14\sin(2\pi x), \tag{43}$$

$$\frac{dR_{f\pm}}{dx} = \frac{dR_{a\pm}}{dx} = \frac{dR_{s-}}{dx} = \frac{DR_0}{dx} = 0, \tag{44}$$

and $(\rho, p, u_x, u_y, u_z, B_y, B_z)$ is (1.0, 0, −0.5, 0, 0, 3.0, 2.0) at $x = 0$. Here, $R_0 \equiv pV^\gamma$, $B_x = 3.0$. Wave speeds for fast, Alfven, and slow waves under the initial condition are around 1.53, 0.846, and 0.506. We measure the convergence by the difference between the converged solution and the solution after each iteration:

$$\begin{aligned}\varepsilon_{1d} = {} & \frac{1}{p_0 L}\sum_{i=1}^{N}\Delta x_i^{(n)}[|P_i^{(n)} - P_{i,*}^{(n)}| + |P_{yi}^{(n)} - P_{yi,*}^{(n)}| + |P_{zi}^{(n)} - P_{zi,*}^{(n)}|] \\ & + \frac{1}{c_0 L}\sum_{i=1}^{N}\Delta x_i^{(n)}[|u_{xi}^{(n)} - u_{xi,*}^{(n)}| + |u_{yi}^{(n)} - u_{yi,*}^{(n)}| + |u_{zi}^{(n)} - u_{zi,*}^{(n)}|] \\ & + \frac{1}{p_0 L}\sum_{i=1}^{N}\Delta x_i^{(h)}[|P_i^{(h)} - P_{i,*}^{(h)}| + |P_{yi}^{(h)} - P_{yi,*}^{(h)}| + |P_{zi}^{(h)} - P_{zi,*}^{(h)}|] \\ & + \frac{1}{c_0 L}\sum_{i=1}^{N}\Delta x_i^{(h)}[|u_{xi}^{(h)} - u_{xi,*}^{(h)}| + |u_{yi}^{(h)} - u_{yi,*}^{(h)}| + |u_{zi}^{(h)} - u_{zi,*}^{(h)}|].\end{aligned}$$

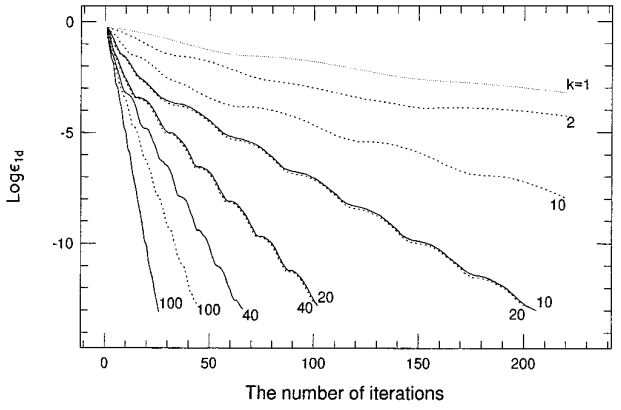

FIG. 7. A difference between the converged solution and the solution after each iteration for ideal MHD equations, with 200 cells in [0, 1], $\Delta t = 0.394966$. Courant numbers associated with fast, Alfven, and slow waves are about 120, 67, and 40. The dotted line is obtained from $\mathbf{A}_1$, dashed lines are obtained from $\mathbf{A}_k$ for $k = 2$, 10, 20, 40, and 100, and solid lines are obtained from $\mathbf{B}_k$ for $k = 10$, 20, 40, and 100.

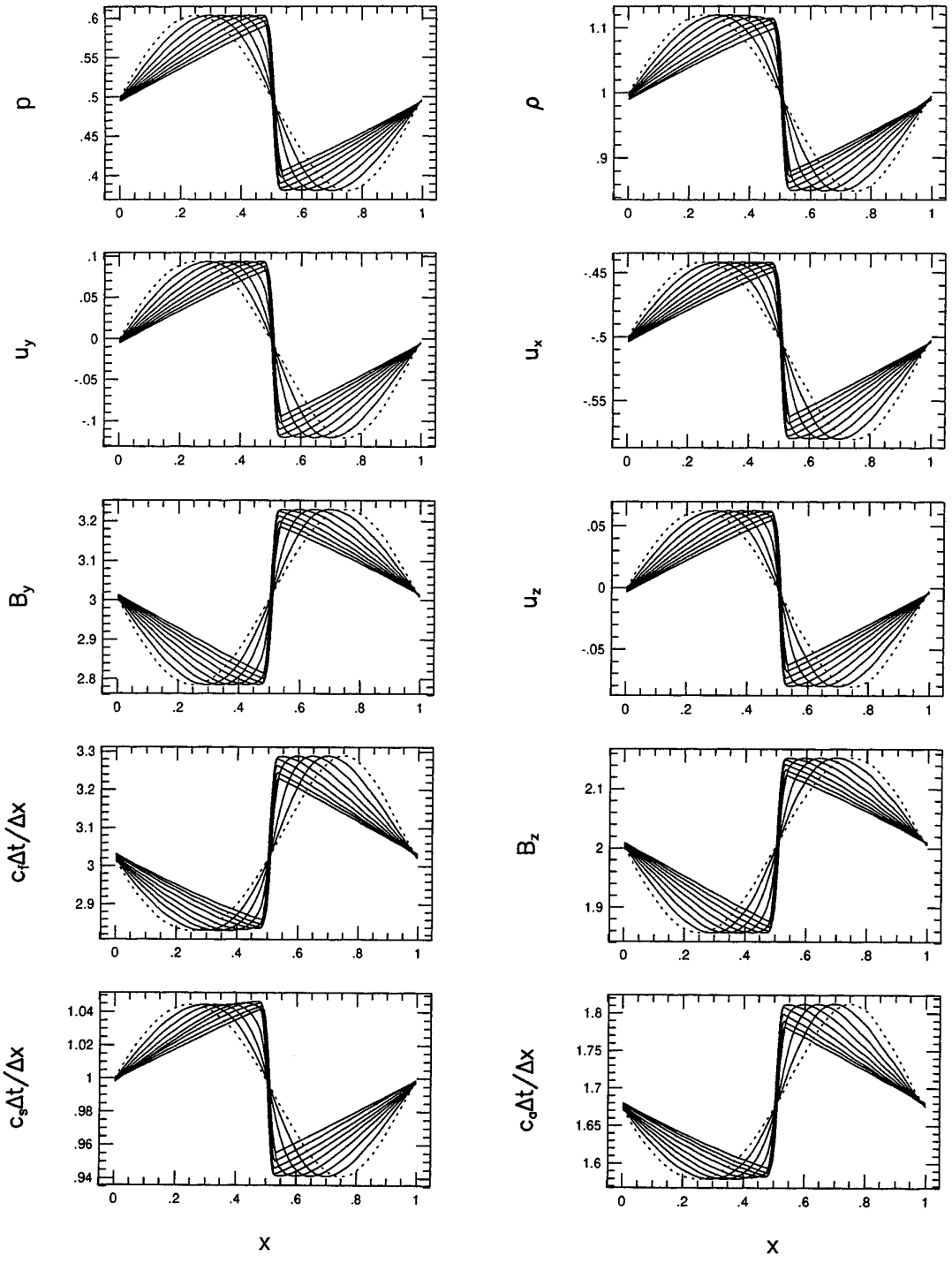

FIG. 8. The propagation of a slow wave: $B_x = 3$, 200 cells in [0, 1], $\Delta t = 9.87417 \times 10^{-3}$, and $\mathbf{B}_{25}$ and 3 iterations. Solid lines are the profiles at $t = 0.5$, 1.0, 1.5, 2.0, 2.5, 3.0, 3.5, and 4.0.

Here p_0 and c_0 are the thermal pressure and sound speed at $x = 0$, the subscript $*$ stands for the converged solution, and $\Delta x_i^{(n)}$ and $\Delta x_i^{(h)}$ are the widths of the ith cell in the Lagrangian grid at $t = \Delta t$ and $\Delta t/2$.

The dotted line in Fig. 7 shows the relation between ε_{1d} and the number of iterations obtained from $\mathbf{A}_1$ when a uniform grid with N (= 200) numerical cells are used in [0, 1], and $\Delta t = 0.39498$. Courant numbers associated with

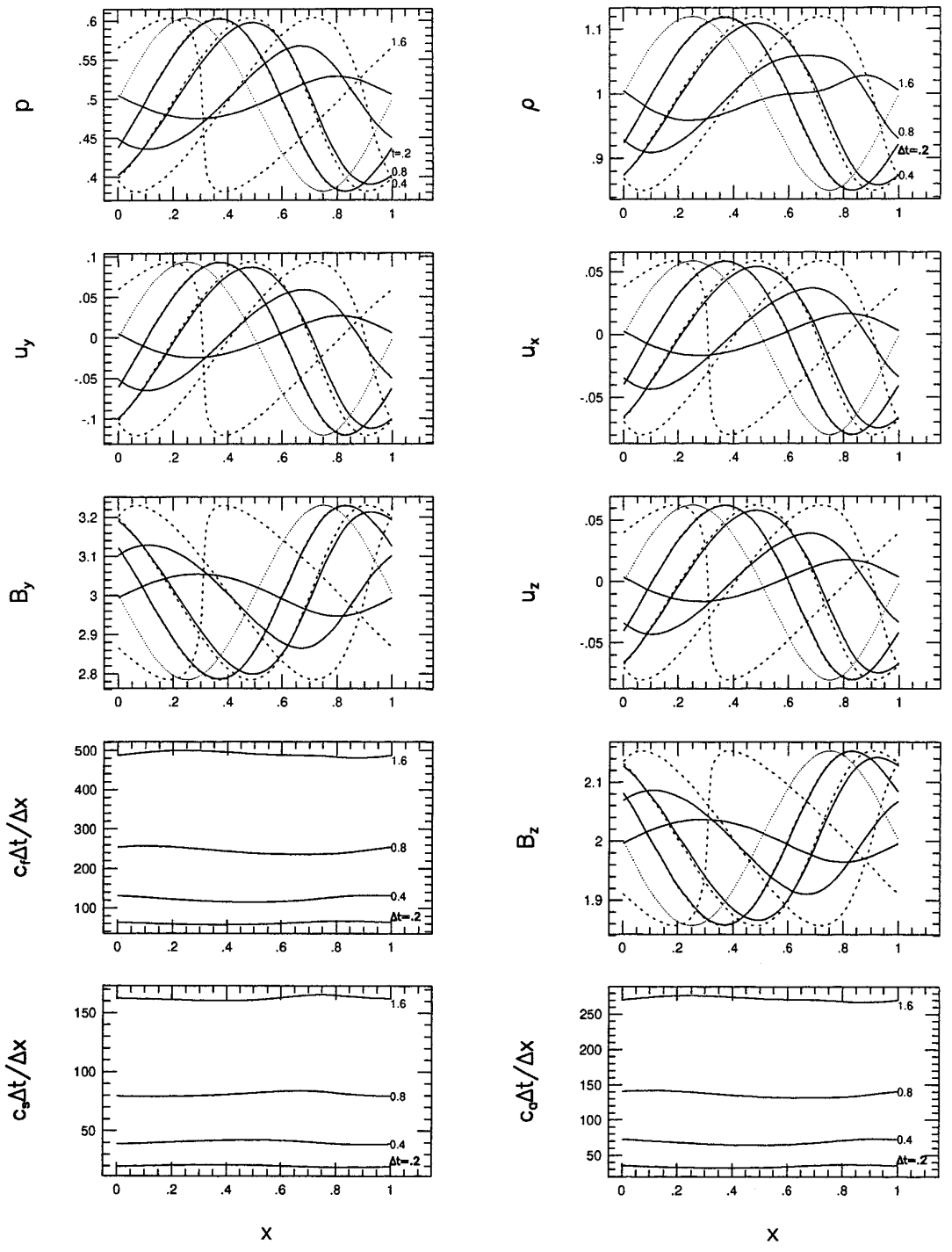

FIG. 9. A slow wave (solid lines) after one time step when different time steps are used: 200 cells in [0, 1] and $\mathbf{B}_{50}$. Dotted lines are the initial condition. The numbers in the upper-right box are $\Delta t = 0.2$, 0.4, 0.8, and 1.6, and they are for the solutions from the hybrid scheme (solid lines). Dashed lines are references obtained from an explicit scheme. The numbers in the upper-left box indicate the solution from the explicit scheme at different times, i.e., $t = 0.2$, 0.4, 0.8, and 1.6. The numbers of iterations used here are the following: 6 iterations for $\Delta t = 0.2$; 10 iterations for $\Delta t = 0.4$; 14 iterations for $\Delta t = 0.8$; and 24 iterations for $\Delta t = 1.6$.

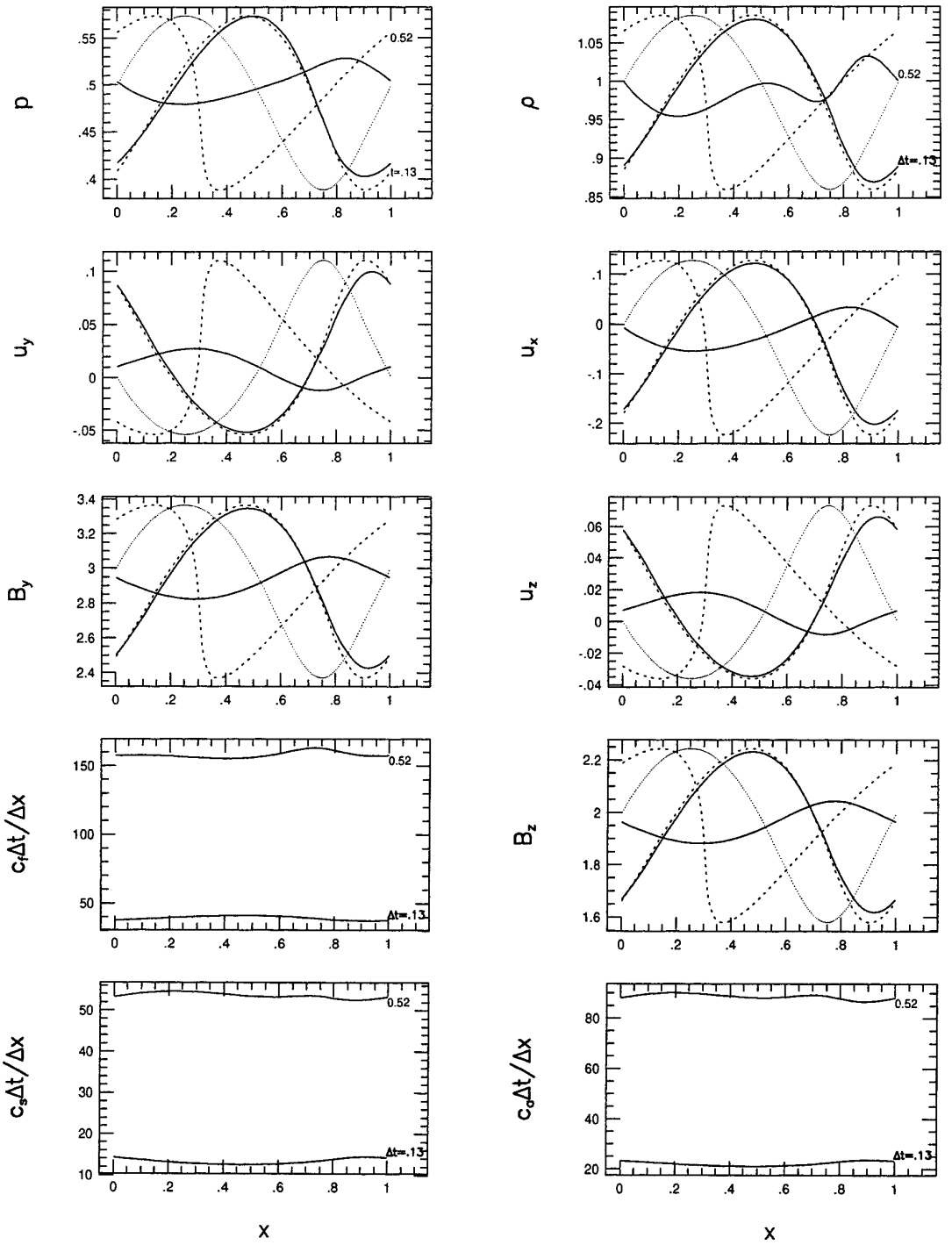

FIG. 10. A fast wave (solid lines) after one time step when time steps $\Delta t = 0.13$ and 0.52 are used, with 200 cells in [0, 1] and $\mathbf{B}_{50}$. Dotted lines are the initial condition. The numbers in the upper-right box are $\Delta t = 0.13$ and 0.52, and they are for the solutions from the hybrid scheme (solid lines). Dashed lines are solutions obtained from an explicit scheme at $t = 0.13$ and 0.52, which are indicated by the numbers in the upper-left box. The number of iterations used here is the following: 12 iterations for $\Delta t = 0.13$ and 18 iterations for $\Delta t = 0.52$.

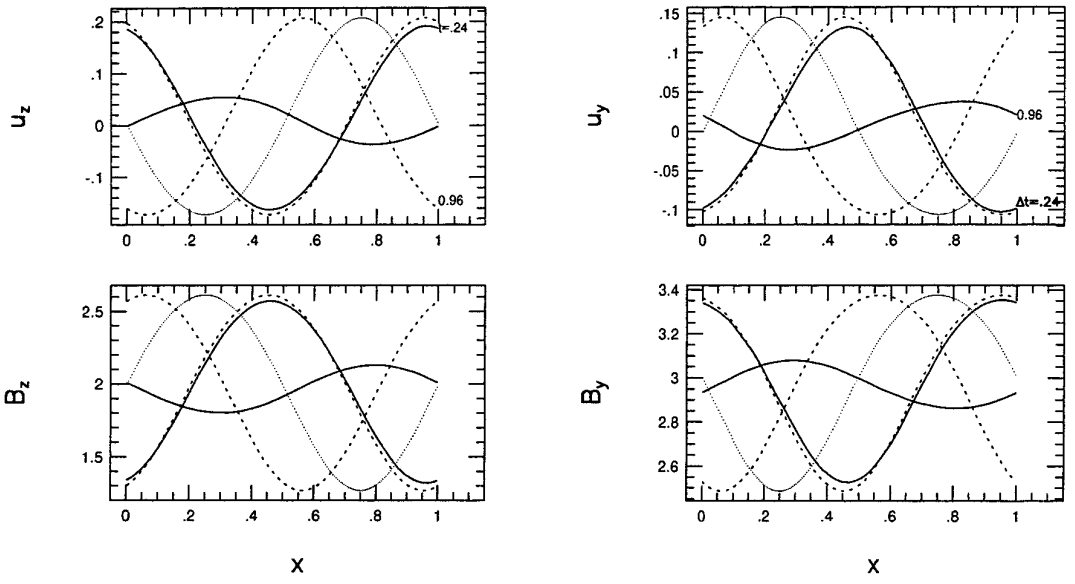

FIG. 11. An Alfven wave (solid lines) after one time step when time steps $\Delta t = 0.24$ ($\approx 40\ \Delta x/c_a$) and 0.96 ($\approx 160\ \Delta x/c_a$) are used, with 200 cells in [0, 1] and $\mathbf{B}_{50}$. Dotted lines are the initial condition. The numbers in the upper-right box are $\Delta t = 0.24$ and 0.96, which are for the solutions from the hybrid scheme (solid lines). The numbers in the upper-left box are $t = 0.24$ and 0.96, which are for the solutions from an explicit scheme (dashed lines). The number of iterations used here is the following: 10 iterations for $\Delta t = 0.24$ and 18 iterations for $\Delta t = 0.96$.

fast, Alfven, and slow waves, $c_f\ \Delta t/\Delta x$, $c_a\ \Delta t/\Delta x$, and $c_s\ \Delta t/\Delta x$, are around 122, 67.6, and 40.4 respectively. It is $c_f\ \Delta t/\Delta x$ that cannot be larger than unity in an explicit scheme. The convergences obtained from the approach $\mathbf{A}_k$ for $k = 2$, 10, 20, 40, and 100 are given by the dashed lines in Fig. 7, and the convergences obtained from the approach $\mathbf{B}_k$ for $k = 10$, 20, 40, and 100 are given by solid lines in Fig. 7.

The first example for ideal MHD equations is the propagation of a slow wave initially given by Eqs. (43), (44) with a shifted flow velocity u_x. The initial condition is shown by the dotted lines in Fig. 8. At each time step, fast and Alfven waves are implicitly treated, and slow waves are partially implicitly and partially explicitly treated. Figure 9 shows the feature of the scheme for the slow wave when different time steps are used. The dotted lines in the figure are the initial condition, and dashed lines are considered as references which are obtained from an explicit scheme [26]. It is hard to see the difference between the implicit and explicit schemes when $\Delta t = 0.1$ ($\approx 20\ \Delta x/c_s$).

In order to show the property of the scheme for fast (or Alfven) waves, we initially set up a fast (or an Alfven) wave through a nonvanishing differential of Riemann invariant dR_{f+} (or dR_{a+}) and set (ρ, p, u_x, u_y, u_z, B_y, B_z) to (1.0, 0, -0.5, 0, 0, 3.0, 2.0) at $x = 0$. $B_x = 3.0$. The solid lines in Fig. 10 show a fast wave after one time step when $\Delta t = 0.13$ ($\approx 40\ \Delta x/c_f$) and $\Delta t = 0.52$ ($\approx 160\ \Delta x/c_f$) are used. The solid lines in Fig. 11 show a Alfven wave after one time step when $\Delta t = 0.24$ ($\approx 40\ \Delta x/c_a$) and $\Delta t = 0.96$ ($\approx 160\ \Delta x/c_a$) are used.

We do not recommend the use of an implicit scheme for shock-tube problems. If a discontinuity has to be resolved in some part of a simulation domain, sizes of time steps should be restricted so that Courant numbers corresponding to the wave in that part of the domain remain around unity. Figure 12 shows the solution of a shock-tube problem obtained from the implicit–explicit scheme. In order to resolve well the slow shocks and rotational discontinuities before they travel beyond the simulation domain, we have used 800 cells in [0, 1] for this problem. Solid lines in Fig. 12 show the profiles at $t = 0.7$. The solution of the shock tube problem contains two rotational discontinuities, two slow shocks, and one contact discontinuity. The structure near $x = 0$ in the density profile comes from the pure discontinuity in the initial condition, and it may be reduced through a very small structure introduced for the initial discontinuity [26].

5. CONCLUSIONS AND DISCUSSIONS

We have developed an iterative implicit–explicit hybrid scheme for hyperbolic systems of conservation laws. The scheme is of Godunov-type in both implicit and explicit regimes, in which the flux needed in a Godunov scheme is calculated from Riemann problems, is accurate to second order in both space and time for all Courant numbers, is in a strictly conservation form, and is able to resolve discontinuities. Each wave in the scheme may be either implicitly, or explicitly, or partially implicitly and partially explicitly treated depending on its associated Courant

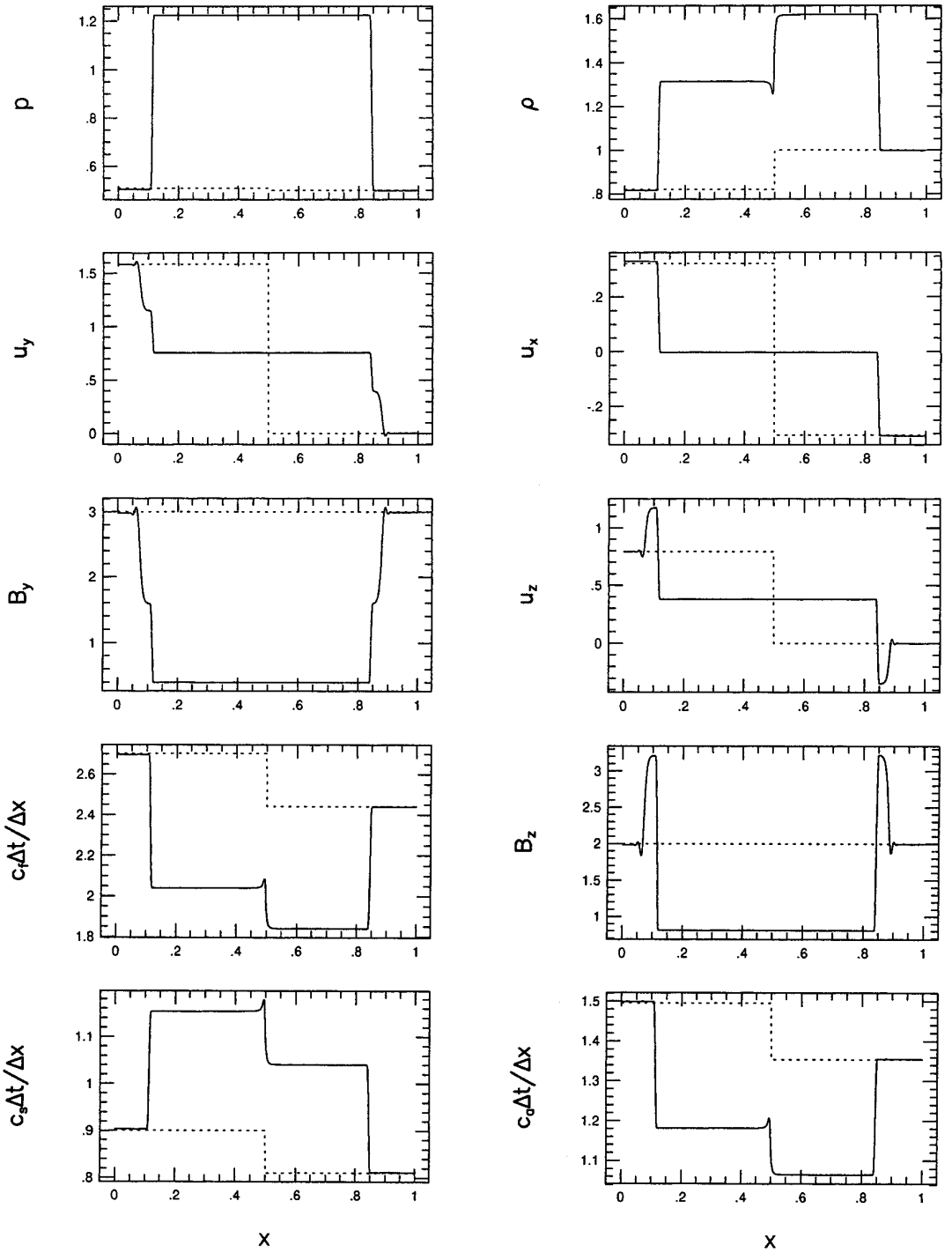

FIG. 12. A shock tube problem, with $\Delta t = 0.002$, 800 cells in [0, 1], and $\mathbf{B}_{100}$ and 3 iterations. Initially, $(\rho, p, u_x, u_y, u_z, B_y, B_z)$ is (0.82, 0.509, 0.3235, 1.586, 0.7946, 3, 2) for $x < 0.5$, and (1, 0.5, −0.3052, 0, 0, 3, 2) for $x > 0.5$. $B_x = 3$. The initial condition is shown by the dashed lines. The solid lines are the profiles at $t = 0.7$, which contain two slow shocks, two rotational discontinuities, and one contact discontinuity.

number in each numerical cell, and the scheme is able to smoothly switch between implicit and explicit calculations. Only a single level of iterations is involved in the scheme, which solves both the implicit relations arising from upstream centered differences for all wave families and the nonlinearity of a system. The multicolors proposed in the paper may reduce the number of iterations required to reach a converged solution for a large time step by several orders. Compared to the largest Courant number in a simulation with large time steps, only a small number of iterations are needed in the scheme. The computer code of the scheme is easy to vectorize.

The feature of the scheme has been shown through numerical examples for the Euler equations and ideal MHD equations. The shorter wavelength modes undergo the stronger damping, for a given wavelength the solution approaches the correct steady state in the limit of large Courant number, and significant phase errors develop only for Courant numbers for which there is strong damping. The scheme has advantages for the problems in which accuracy is important in at least some part of a simulation domain and has special advantages for the problems in which the accuracy is important for waves with relatively small wave speeds.

There are two points we would like to discuss here. First, practical problems normally involve more physical effects than those included in Eq. (12). The terms, which are not included in Eq. (12), but are included in a more complete set of physical equations, may be treated through an operator splitting technique. These additional terms may be explicitly treated after the dynamical step described in this paper. Second, most practical problems involve multidimensions. The extension of the scheme to multidimensional hyperbolic systems of conservation laws is extremely desirable and is very important for the practical value of the scheme.

ACKNOWLEDGMENTS

This work was supported by the National Science Foundation under Grant NSF-ASC-9309829, the Department of Energy under Grant DE-F602-87ER25035, the Laboratory for Computational Science and Engineering, and the Minnesota Supercomputer Institute.

REFERENCES

1. S. K. Godunov, *Math. Sb.* **47,** 271 (1959).
2. B. Van Leer, *J. Comput. Phys.* **23,** 276 (1977).
3. B. Van Leer, *J. Comput. Phys.* **32,** 101 (1979).
4. P. L. Roe, *J. Comput. Phys.* **43,** 358 (1981).
5. P. R. Woodward and P. Colella, *Lecture Notes Phys.* **141,** 434 (1981).
6. P. Colella and P. R. Woodward, *J. Comput. Phys.* **54,** 174 (1984).
7. A. Harten, *J. Comput. Phys.* **49,** 359 (1983).
8. H. B. Keller and P. R. Wendroff, *Comm. Pure Appl. Math.* **10,** (1957), 567.
9. S. Nakamura, *Computational Method in Engineering and Science* (Wiley, New York, 1976), pp. 175–187.
10. R. W. Beam and R. F. Warming, *J. Comput. Phys.* **22,** 87 (1976).
11. B. Engquist and S. Osher, *Math. Comp.* **34,** 45 (1980).
12. B. Van Leer and W. A. Mulder, in *Numerical Methods for the Euler Equations of Fluid Dynamics*, edited by F. Angrand, A. Dervieux, J. A. Desideri, and R. Glowinski, (SIAM, Philadelphia, PA, 1985), p. 312.
13. H. C. Yee, R. F. Warming, and A. Harten, *J. Comput. Phys.* **57,** 327 (1985).
14. H. M. Glaz and A. B. Wardlaw, *J. Comput. Phys.* **58,** 157 (1985); **12A,** 413 (1986).
15. B. A. Fryxell, P. R. Woodward, P. Colella, and K.-H. Winkler, *J. Comput. Phys.* **63,** 283 (1986).
16. A. Jameson and S. Yoon, *AIAA J.* **24,** 1737 (1986).
17. A. Jameson and S. Yoon, *AIAA J.* **25,** 929 (1987).
18. C. Y. Loh and W. H. Hui, *J. Comput. Phys.* **89,** 207 (1990).
19. M. Blunt and B. Rubin, *J. Comput. Phys.* **102,** 194 (1992).
20. M. Wilcoxson and V. Manousiouthakis, *J. Comput. Phys.* **115,** 376 (1994).
21. J. P. Collins, P. Collela, and H. M. Glaz, *J. Comput. Phys.* **116,** 195 (1995).
22. W. Dai and P. R. Woodward, *J. Comput. Phys.*, **124,** 217 (1996).
23. J. E. Fromm, *J. Comput. Phys.* **3,** 176 (1968).
24. G. A. Sod, in *Numerical Methods in Fluid Dynamics* (Cambridge Univ. Press, Cambridge, 1985), p. 155.
25. L. D. Landau and E. Lifshits, *Electrodynamics of Continuous Media*, Pergamon, New York, 1960.
26. W. Dai and P. R. Woodward, *J. Comput. Phys.* **121,** 51 (1995).
27. R. Courant and K. O. Friedrichs, *Supersonic Flow and Shock Wave*, 5th ed., Interscience, New York, 1967.
28. H. R. Strauss, *Phys. Fluids* **19,** 134 (1976).
29. H. R. Strauss, *Phys. Fluids* **20,** 1354 (1977).
30. J. U. Brackbill, in *Methods in Computational Physics*, edited by J. Killeen, Vol. 16 (Academic Press, New York, 1976), p. 1.
31. C. H. Finan and J. Killeen, *J. Comput. Phys.* **24,** 441 (1981).
32. A. Y. Aydemir and D. C. Barnes, *J. Comput. Phys.* **53,** 100 (1984).
33. A. Y. Aydemir and D. C. Barnes, *J. Comput. Phys.* **59,** 108 (1985).
34. D. S. Harned and W. Kerner, *J. Comput. Phys.* **60,** 62 (1985).
35. D. S. Harned and D. D. Schnack, *J. Comput. Phys.* **65,** 57 (1986).
36. D. D. Schnack, D. C. Barnes, and Z. Mikic, *J. Comput. Phys.* **70,** 330 (1987).
37. L. A. Charlton, J. A. Holmes, V. E. Lynch, B. A. Carreras, and T. C. Hender, *J. Comput. Phys.* **86,** 270 (1990).
38. K. Lerbinger and J. F. Luciani, *J. Comput. Phys.* **97,** 444 (1991).